Title: Strike-slip Faulting During the 2014 Bárðarbunga-Holuhraun Dike Intrusion, Central Iceland.

Authors: Thorbjörg Ágústsdóttir[1,]*†, Jennifer Woods[1]†, Tim Greenfield[1], Robert G. Green[1], Robert S. White[1,2], Tom Winder[1], Bryndís Brandsdóttir[2], Sveinbjörn Steinthórsson[2], Heidi Soosalu[3]

Affiliations:

[1]Bullard Laboratories, Department of Earth Sciences, University of Cambridge, Madingley Road, Cambridge, CB3 0EZ, UK.

[2]Institute of Earth Sciences, University of Iceland, Askja, Sturlugata 7, 101 Reykjavík, Iceland.

[3]Geological Survey of Estonia, Kadaka tee 82, 12618 Tallinn, Estonia.

†The first two authors contributed equally to this paper.

*Correspondence to: ta354@cam.ac.uk

Accepted Article

This article has been accepted for publication and undergone full peer review but has not been through the copyediting, typesetting, pagination and proofreading process which may lead to differences between this version and the Version of Record. Please cite this article as doi: 10.1002/2015GL067423

©2016 American Geophysical Union. All rights reserved.

Abstract:

Over a 13 day period magma propagated laterally from the sub-glacial Bárðarbunga volcano in the northern rift zone, Iceland. It created > 30,000 earthquakes at 5–7 km depth along a 48 km path before erupting on 29 August 2014. The seismicity, which tracked the dike propagation, advanced in short bursts at 0.3–4.7 km/h separated by pauses of up to 81 hours. During each surge forward, seismicity behind the dike tip dropped. Moment tensor solutions from the leading edge show exclusively left-lateral strike-slip faulting sub-parallel to the advancing dike tip, releasing accumulated strain deficit in the brittle layer of the rift zone. Behind the leading edge, both left- and right-lateral strike-slip earthquakes are observed. The lack of non double-couple earthquakes implies that the dike opening was aseismic.

Key points:

Magma propagated 48 km laterally at 5–7 km below sea level prior to erupting, generating > 30,000 earthquakes

Seismicity arises from double-couple strike-slip failure orientated sub-parallel to the dike strike

Left-lateral fault motion is dominant to accommodate extension across the divergent plate boundary

Keywords:

Dike propagation, dike tip fracture, earthquake mechanisms, rifting, Bárðarbunga, Holuhraun

Accepted Article

©2016 American Geophysical Union. All rights reserved.

1. Introduction

Volcanic eruptions in rift zones are frequently preceded by lateral migration of a magma-filled dike, sometimes for many kilometers [*e.g. Rubin and Pollard*, 1988; *Rubin*, 1992; *Belachew et al.*, 2011]. Some of these dike intrusions freeze at depth while others breach the surface, resulting in a fissure eruption [e. g. *Björnsson and Saemundsson*, 1977; *Abdallah et al.*, 1979; *Hamling et al.*, 2009; *Wright et al.*, 2012]. Seismicity often accompanies propagation of the dike front as the magma forces its way forward [*Einarsson and Brandsdóttir*, 1978; *Brandsdóttir and Einarsson*, 1979; *Battaglia et al.*, 2005; *Morita et al.*, 2006; *Keir et al.*, 2009], commonly fed by a subsiding volcanic center [e.g. *Einarsson and Brandsdóttir*, 1978]. The extent of accompanying seismicity is variable, influenced strongly by the pre-existing stresses and material properties of the rift fabric [*Rubin and Gillard*, 1998; *Rivalta et al.*, 2015]. However, when seismicity is present the migrating earthquake swarm marks the tip of the intrusion [*Brandsdóttir and Einarsson*, 1979; *Grandin et al.*, 2011].

The Bárðarbunga volcanic system is made up of a sub-glacial central volcano with an ice-filled caldera and a transecting fissure swarm which extends 115 km SW (the Veiðivötn fissure swarm) and 55 km NNE (the Dyngjuháls fissure swarm) [*Jóhannesson and Saemundsson*, 1998; *Larsen et al.*, 2013; *Larsen and Gudmundsson*, 2015]. Episodic rifting within the fissure swarms of Icelandic volcanoes accommodates plate spreading along the divergent plate boundary [*Tryggvason*, 1984; *Wright et al.*, 2012]. Gravity studies suggest that dense intrusions have previously radiated at depth from the Bárðarbunga central volcano [*Gudmundsson and Högnadóttir*, 2007].

In 2014 a dike propagated laterally 48 km from Bárðarbunga central volcano north-east along the Dynguháls fissure swarm. After 13 days propagation the dike erupted at

©2016 American Geophysical Union. All rights reserved.

Accepted Article

Holuhraun, reoccupying old craters formed before the mid-nineteenth century by magma which also originated within the Bárðarbunga system [*Hartley and Thordarson*, 2013]. This study addresses the origin and extent of migrating seismicity accompanying the 2014 dike intrusion. The spatio-temporal resolution exceeds that of numerous previous observations of dike seismicity [*Passarelli et al., 2015; Rivalta et al., 2015 and references therein*]. We assess the relationship between the dike trajectory and seismicity, and construct precise fault plane solutions to investigate the failure mechanisms along the dike.

1.1. The 2014 Bárðarbunga-Holuhraun Dike Intrusion

On 16 August 2014 an unusual sequence of earthquakes began near the south-eastern rim of the ice-covered Bárðarbunga caldera. The earthquakes migrated rapidly 6 km south-eastwards, delineating a laterally propagating, radial dike, before turning 90° north-eastwards away from the caldera. Over the next twelve days the dike propagated episodically a further 42 km beneath the glacier and into the Holuhraun lava field. It advanced beyond the eventual eruption site by 2 km, making the total length of the dike 48 km (Figure 1, Movie S1). It was not until 29 August that the dike breached the surface, reoccupying the old Holuhraun craters. The initial fissure eruption lasted only 4 h. A further 40 h later, on 31 August, a sustained and larger fissure eruption began. It continued until 27 February 2015, erupting 1.6 km^3 of lava over an area of 84.1 km^2 [*Gíslason et al.*, 2015].

The dike propagation followed a pathway of minimum potential energy [*Heimisson et al.*, 2015; *Sigmundsson et al.*, 2015a]. Five large-scale segments can be identified, each distinguishable by a change in dike strike (Figures 1 and 2). The strike of the northernmost dike segment in the ice-free region is 025°, consistent with the regional rift fabric orientation of 025º [*Hjartardóttir et al.*, 2015a] but 11° clockwise from the normal to the plate spreading direction of 104°, extending at 18.5 mm/y [*DeMets et al.*, 2010]. Surface fracturing and

©2016 American Geophysical Union. All rights reserved.

graben formation accompanied the intrusion [*Hjartardóttir et al.*, 2015b]. Modeling of geodetic data shows that it was a vertically-extensive planar dike [*Green et al.*, 2015; *Sigmundsson et al.*, 2015a]. During the dike propagation Bárðarbunga caldera began to subside and experienced over 50 M>3 earthquakes, suggesting a deflating magma reservoir beneath the caldera.

2. Seismic Data

A seismic network deployed by Cambridge University has been operated in Iceland since 2006 and expanded to surround Vatnajökull icecap in 2013. In August 2014 the network comprised 72 three-component broadband seismometers (Figures 1 and S1) that recorded the 2014 Bárðarbunga-Holuhraun dike propagation in detail. To complement the network, 14 stations from the national seismic network of the Icelandic Meteorological Office were used, as well as one British Geological Survey station and one University College Dublin station. The network provides good azimuthal coverage, with excellent sampling north of the ice cap. Coverage is less good to the south of the dike due to difficult field conditions on the icecap. The data used in this study covers the period from 16 to 31 August 2014, encompassing the whole dike intrusion and the onset of the two eruptions. All data were recorded at 100 Hz sample rate with a GPS time stamp.

More than 30,000 earthquakes (M_L 0.5–4) were automatically detected by Coalescence Microseismic Mapping [*Drew et al.*, 2013]. Accurate hypocenter locations were determined using NonLinLoc [*Lomax et al.*, 2000], with average location errors of 0.5 km laterally and 1.0 km in depth. We used a linear gradient velocity model for earthquake locations based on refraction experiments [*Pálmason*, 1971; *Gebrande et al.*, 1980; *Darbyshire et al.*, 1998] with a constant Vp/Vs ratio of 1.78, constrained by the Wadati-plots [*Wadati*, 1933] from manually picked phase arrival times along the whole dike (Figure S2,

©2016 American Geophysical Union. All rights reserved.

Accepted Article

Table S1).

A manually constructed earthquake catalogue was created by refining earthquake arrival times for more than 500 events, producing 30,000 P-phase and 28,000 S-phase picks. Refined earthquakes were located with NonLinLoc to determine earthquake hypocenters with average errors of 0.5 km laterally and 0.9 km in depth (Figures 1, S2 and Table S3).

3. Bárðarbunga-Holuhraun Dike Seismicity

3.1. Seismicity Migration

During the intrusion new segments of the Bárðarbunga-Holuhraun dike were emplaced in propagation phases at speeds of 0.3–4.7 km/h, with seismicity focused around the dike tip. The advances were separated by periods where the migration stalled for up to 81 h. During periods of most rapid propagation, quiet zones occurred immediately behind the concentrated seismicity of the leading edge. The propagation phases are delineated by tight clusters in space and time of advancing earthquakes, highlighted by grey bands in Figure 2a. They last between 40 min and 13 h, with the longest continuous advance of 5.5 km made in 13 h. Large-scale dike segments were emplaced by episodic intrusion of many smaller segments with similar orientations. Each of the main segments became seismically quiet once a new segment had intruded beyond it, producing the step-like propagation of seismicity apparent in Figure 2a.

3.2. Seismicity Distribution

Throughout the dike emplacement, seismicity remained concentrated at 5–7 km below sea level, near the brittle-ductile boundary where differential stresses in this extensional area are greatest. The brittle-ductile boundary is mapped at about 7 km depth in the Askja volcanic system, located about 20 km along rift from the dike tip [*Key et al.*, 2011a,b *Green et al.*, 2014]. Sparse seismicity was observed in the uppermost four kilometers of crust at several

©2016 American Geophysical Union. All rights reserved.

Accepted Article

sub-glacial locations (stars on Figure 1), but none near the eruption fissure, despite the dike breaching the surface. Persistent seismicity was observed at discrete locations along the dike, appearing as horizontal bands of seismicity on a distance-along-dike versus time plot (Figures 2a-b). A cluster at 37.5 km (64.80°N) occurred where the dike stalled for 14 h before surging forward. Another cluster is seen at 46 km (64.87°N), below the southern edge of the eruption fissure (Figures 2a–b).

3.3. Seismicity Rates and Moment Release

The majority of the seismic moment release accompanying intrusion of the Bárðarbunga-Holuhraun dike occurred during the rapid propagation phases (grey bands in Figure 2a). The largest increase in the moment release occurred simultaneously with the rapid advance of the dike on 24 August. Between propagation phases seismicity rates generally remained high but smaller magnitude earthquakes were observed. On several occasions the seismicity retreated or appeared to back-propagate, such as following the onset of the initial fissure eruption. In this case the seismicity rate remained high but immediately retreated ~8 km along the dike, before migrating back to the eruption site over the subsequent 8 h. An instantaneous drop in seismicity rate along the entire dike was observed with the onset of the main eruption on 31 August (Figure 2).

3.4. Earthquake Source Mechanisms

In order to investigate the earthquake source mechanisms we concentrate on the 13 km of the dike nearest the eruption site (red box Figure 2a, beyond 64.78°N, emplaced from 24 August 2014). This northernmost segment of the dike has a strike of 025º and is where the seismic network provides the best azimuthal and spatial constraints. Lower hemisphere fault plane solutions and inversions of the full moment tensor were constructed using a Bayesian moment tensor solution program MTINV [*Pugh,* 2015]. Each event had a minimum distance to the nearest station of 1–7 km, a maximum azimuthal gap of 30°–50°, and an average of 53

©2016 American Geophysical Union. All rights reserved.

Accepted Article

P-phase polarities (Figure 3). Inversions for the full moment tensor revealed no significant volumetric component, despite the setting of an opening dike. All fault plane solutions are best described by double-couple failure. There is a surprising lack of normal faulting events, given this is an extensional rift setting (Figure S3). Instead, we find that the dominant failure mechanism is strike-slip. One nodal plane is consistently sub-parallel to the strike of the dike so we assume this to be the fault plane (Figures 4a–b). There is a significant range in the dike-perpendicular nodal plane orientations (Figure 3), strongly suggesting that they are not fault planes. It is therefore most likely that the fractures generated during the 48 km dike propagation are sub-parallel to the direction of travel.

The fault plane solutions constrain populations of left- and right-lateral strike-slip mechanisms with consistent fault planes (Figures 4a–b). The strike of the average left-lateral fault plane solution is 038° (Figure 4a, green on Figure S3b). This is a rotation of 13º clockwise from the strike of the dike and the regional rift orientation of ~025º [*Hjartardóttir et al.*, 2015a]. The right-lateral faulting observed occurs predominantly behind the leading edge, mainly in a cluster at 46 km (64.87°N) near the southern edge of the eruption fissure (red on Figure S3b). The strike of the average fault plane solution for this population is 017° (Figure 4b). The distribution of fault plane strikes is shown in the rose diagrams in Figures 4a-b.

3.5. Earthquake Fault Motion Categorization

A categorization method based on the consistency of the nodal planes (described above) was used to analyse the earthquake failure mechanisms in the northernmost dike segment (Figure 2b). Two representative sets of stations from opposite polarity quadrants (dilatational and compressional) were selected with reliable, clear arrivals and stable locations on the focal sphere. Hence, plotting the earthquake arrival waveforms for both sets of 7 stations enabled quick differentiation between left- and right-lateral fault motion (Figure

©2016 American Geophysical Union. All rights reserved.

Accepted Article

S4). Results from manually constructed fault plane solutions are consistent with the categorization (Figures 2b and S3b), allowing for the rapid failure mechanism analysis of ~9500 events.

The fault motion categorization shows that the principal failure mechanism along the dike is left-lateral strike-slip (85%, green on Figures 2b–c). Right-lateral strike-slip faulting is less common (15%, red on Figures 2b–c). The leading edge failure is exclusively left-lateral strike-slip. Right-lateral strike-slip failure only occurs after the leading edge of the dike has passed, persistently in a cluster at the southern end of the eruptive fissure, 1 km shallower than the majority of the seismicity (Figure 2c). Uncategorized earthquakes (grey on Figures 2b–c) are generally those with signal to noise ratios too low to confidently identify first motion polarities.

4. Discussion

As in other intrusions [*Brandsdóttir and Einarsson*, 1979; *Keir et al.*, 2009; *Belachew et al.*, 2011; *Grandin et al.*, 2011] the seismicity was confined to the region close to the front of the propagating dike, suggesting that the flow of magma is aseismic once a pathway has formed and remains open. The quiet zones observed immediately behind the leading edge during rapid propagation phases (grey bands on Figure 2b) may be due to stress shadowing [*Segall et al.*, 2013]. During the stalled phases a resupply of magma by lateral flow from Bárðarbunga volcano inflated the region behind the dike tip and allowed the pressure to build up sufficiently to drive the next advance forward [*Sigmundsson et al.*, 2015a]. The initial eruption on 29 August may have been short lived because it used up all the magma available in the dike and the pressure dropped. It then took two days for a consistent magma supply channel to form between the source and the fissures, before the start of the main, continuous eruption. Locations of persistent seismicity along the dike, behind the leading edge, may be due to an increase in local strength of the surrounding medium which required continual

©2016 American Geophysical Union. All rights reserved.

Accepted Article

fracturing to maintain magma flow. Equally, they could arise from angular jogs in the dike, such as at the southern end of the eruptive fissure where magma moves upward to the eruption fissure.

During emplacement, dike seismicity remained at 5–7 km depth. However, surface geodetic observations require most of the opening to be above 5 km depth [*Green et al.*, 2015; *Sigmundsson et al.*, 2015a]. The dike certainly extended shallower than the seismicity at the eruption fissure at Holuhraun. Small magma volumes may also have reached the surface at several other sub-glacial locations, especially where ice depressions formed at the surface (orange stars on Figure 1) [*Sigmundsson et al.*, 2015a]. We infer that the uppermost crust is so weak from the pervasive rift fabric that it fractured in tension and the dike inflated largely aseismically as magma was intruded and eventually froze. A similar lack of shallow seismicity was observed during the 1983 Kilauea dike intrusion [*Rubin et al.*, 1998]. Migrating magma in pre-fractured crust may propagate creating little brittle failure as shown by Taisne et al. (2011) where vertical magma propagation at Piton de la Fournaise is associated with fewer and smaller earthquakes than during lateral propagation phases.

Propagation rates vary along the Bárðarbunga-Holuhraun dike from 0.3-4.7 km/h. These speeds of lateral dike propagation, guided by pre-existing fractures, are comparable to those reported from other studies. Measured speeds of magma propagation at Piton de la Fournaise range from 0.7-2.9 km/h [*Battaglia et al.*, 2005; *Peltier et al.*, 2005] and 0.7-2.2 km/h for several rifting events during the 1975-1986 Krafla rifting episode, North Iceland, and the 2005-2010 rifting episode in Dabbahu, East African rift [*Wright et al.*, 2012]. Highest propagation rates are associated with short periods of rapid advance of the dike front on 16, 18 and 23 August.

The dike seismicity arises predominantly from double-couple strike-slip failure, with a minority of oblique normal faults (Figure 2b, S3b). The lack of non double-couple

©2016 American Geophysical Union. All rights reserved.

Accepted Article

earthquakes implies that the opening was aseismic. This is supported by the two orders of magnitude difference between the geodetic moment and seismic moment release of the dike. Seismic moment reflects the brittle energy released by fracturing, whereas geodetic moment records the energy associated with the dike inflation. We calculate the seismic moment to be 1.8×10^{17} Nm and the geodetic moment to be 1.8×10^{19} Nm.

Seismicity along the leading edge of the dike arises exclusively from left-lateral strike-slip failure. These earthquakes exhibit greater seismic moment release than those behind the propagating front, where both left-lateral and right-lateral strike-slip failure is observed. Left-lateral strike-slip failure is the dominant mechanism. This can be explained by the obliquity of the fault planes (038^{o}) to the regional spreading axis (104^{o}). Fault plane motion is preferentially left-lateral to accommodate extension across the divergent plate boundary. The strikes of the fault planes agree with theoretical models of dike tip failure which postulate fracturing oblique to the propagation direction. With a standard coefficient of friction of 0.6, fracturing would be expected ca. 30º to the dike strike, but high fluid pressures can cause greatly reduced fracture angles [*Rubin and Gillard*, 1998]. The high magmatic pressures at the dike tip are sufficient to reduce the angle of failure to 13º clockwise to the dike strike as observed (Figure 4d). Notably, no corresponding right-lateral events are observed along the leading edge on faults oriented 13º anticlockwise to the propagating dike tip. Any faults aligned in that direction would be almost exactly orthogonal to the spreading direction of 104º and may therefore fail aseismically in Mode I failure or at magnitudes smaller than our magnitude of completion (M_c 1.1). Nonetheless, small-scale faulting mapped at the surface close to the fissures shows both left-lateral and right-lateral failure clockwise and anticlockwise to the strike of the dike as predicted by our model [*Hjartardóttir et al.*, 2015b].

Accepted Article

©2016 American Geophysical Union. All rights reserved.

The path of the dike is governed by the pressure field produced by the overlying topographic load and the local stress field [*Sigmundsson et al.*, 2015a]. However, the influence of pre-existing weaknesses must also be considered. Fracture movements on pre-existing faults occur during rifting episodes, and the fracture density in fissure swarms in the northern rift zone gradually increases with time, indicating that dike intrusions tend to use the same pathways many times. The dike unquestionably reoccupied the old Holuhraun craters and the northernmost dike segment is parallel with the surrounding rift fabric [*Hjartardóttir et al.*, 2015a]. Hence, the dike is likely to have followed pre-existing weaknesses within the rift zone.

Throughout the propagation, eruption and cooling phases the seismicity remained concentrated at 5–7 km depth. We therefore infer that after the dike emplacement, an open pathway was formed and magma continued to flow along a conduit at ca. 6 km depth. The primary driving force for the magma flow through the 48 km long dike is likely to be the pressure head from the magma reservoir beneath Bárðarbunga. Effects of magma gas release are assumed to be minimal in the case of lateral sub-horizontal flow. It seems likely that the overburden pressure may have remained too high at the sub-glacial locations where ice depressions formed [*Sigmundsson et al.*, 2015a] for the pressure head available from the magma reservoir to overcome. Instead, the magma migrated north until it reached a topographic low.

The Bárðarbunga caldera subsided 66 m from the beginning to the end of the eruption, accompanied by 79 M > 5 earthquakes [*Sigmundsson et al.*, 2015b]. The subsidence provides a measure of the available driving force for the magma flow. The average flow rate during the 6-month eruption was 100 m^3/s [*Gíslason et al.*, 2015] but at the beginning it was as high as 400 m^3/s [*Pedersen et al.*, 2015], dropping to zero at the end. A simple model of laminar flow through a tube, with an initial flow rate of 400 m^3/s, a driving force of 1.6 MPa

©2016 American Geophysical Union. All rights reserved.

Accepted Article

(65 m thickness of magma with a density of 2500 kg/m^3) and a dynamic viscosity of 100 Pa s, requires a tube of 15 m diameter and a flow rate of 2.3 m/s (8.3 km/h). Using the average eruptive rate of 100 m^3/s and an average driving force of half the magma reservoir thickness (0.8 MPa), a similar size tube of 15.6 m diameter is required, but with a reduced flow rate of 0.8 m/s (2.9 km/h). This is within the bounds of the observed dike front propagation rates of 0.3–4.7 km/h, and suggests that once the flow path has been opened the lateral magma flow can continue unimpeded. The shape of the conduit need not be circular: equivalent flow rates are derived, for example, in rectangular conduits with a width of 7 m and a height of 100 m. Narrow, tall flow channels would fit the geodetic constraints on the extensional width of a few meters for a vertically extensive dike better than a circular channel.

5. Conclusions

The 2014 Bárðarbunga-Holuhraun dike propagated at 5–7 km below sea level, 48 km to the northeast from Bárðarbunga caldera, before erupting at Holuhraun. The propagation was episodic, advancing at velocities of 0.3–4.7 km/h. Seismicity remaining focused around the dike tip and at constrictions or jogs in the dike path. Detailed analysis of the northernmost dike segment reveals that the seismicity arises from double-couple strike-slip failure. Earthquakes along the leading edge are found to be exclusively left-lateral strike-slip failure, which is also the dominant mechanism overall. This preferential fault motion accommodates extension within the rift zone.

Acknowledgments:

Seismometers were borrowed from the Natural Environment Research Council (NERC) SEIS-UK (loans 968 and 1022), with funding by research grants from the NERC and the European Community's Seventh Framework Programme Grant No. 308377 (Project FUTUREVOLC), and graduate studentships from the NERC and Shell. We thank Ágúst Þór Gunnlaugsson and others who assisted with fieldwork in Iceland and Nigel Woodcock for

©2016 American Geophysical Union. All rights reserved.

Accepted Article

helpful discussions. M.T. Gudmundsson, H. Reynolds and Þ. Högnadóttir supplied ice cauldron coordinates. The Icelandic Meteorological Office, Chris Bean (University College Dublin) and the British Geological Survey kindly provided additional data from seismometers in north-east Iceland; data delivery from IMO seismic database 20151001/01. We thank the two anonymous reviewers for constructive comments. Hypocenter locations in Figure 1 are listed in Tables S2 and S3. Department of Earth Sciences, Cambridge contribution number ESC3539.

References :

Abdallah, A., V. Courtillot, M. Kasser, A.-Y. Le Dain, J.-C. Lépine, B. Robineau, J.-C. Ruegg, P. Tapponnier, and A. Tarantola (1979), Relevance of Afar seismicity and volcanism to the mechanics of accreting plate boundaries, *Nature*, *282*(5734), 17–23, doi:10.1038/282017a0.

Battaglia, J., V. Ferrazzini, T. Staudacher, K. Aki, and J.-L. Cheminée (2005), Pre-eruptive migration of earthquakes at the Piton de la Fournaise volcano (Réunion Island), *Geophys. J. Int.*, *161*(2), 549–558, doi:10.1029/2002JB002193.

Belachew, M., C. Ebinger, D. Coté, D. Keir, J. V Rowland, J. O. S. Hammond, and A. Ayele (2011), Comparison of dike intrusions in an incipient seafloor-spreading segment in Afar, Ethiopia: Seismicity perspectives, *J. Geophys. Res. Solid Earth*, *116*(B6), 2156–2202, doi:10.1029/2010JB007908.

Björnsson, A., and K. Saemundsson (1977), Current rifting episode in north Iceland, *Nature*, *266*, 318–323, doi:10.1029/JB090iB12p10151.

©2016 American Geophysical Union. All rights reserved.

Brandsdóttir, B., and P. Einarsson (1979), Seismic activity associated with the September 1977 deflation of the Krafla central volcano in northeastern Iceland, *J. Volcanol. Geotherm. Res.*, *6*, 197–212.

Darbyshire, F. A., I. T. Bjarnason, R. S. White, and Ó. G. Flóvenz (1998), Crustal structure above the Iceland mantle plume imaged by the ICEMELT refraction profile, *Geophys. J. Int.*, *135*(3), 1131–1149.

DeMets, C., R. G. Gordon, and D. F. Argus (2010), Geologically current plate motions, *Geophys. J. Int.*, *181*(1), 1–80, doi:10.1111/j.1365-246X.2009.04491.x.

Drew, J., R. S. White, F. Tilmann, and J. Tarasewicz (2013), Coalescence microseismic mapping, *Geophys. J. Int.*, *195*(3), 1773–1785, doi:10.1093/gji/ggt331.

Einarsson, P., and B. Brandsdóttir (1978), Seismological evidence for lateral magma intrusion during the July 1978 deflation of the Krafla volcano in NE-Iceland, *J. Geophys.*, *47***,** 160-165.

Einarsson, P., and K. Saemundsson (1987), *Í hlutarins eðli, Festschrift for Th. Sigurgeirsson (geological map)*, edited by T. Sigfússon, Menningarsjóður, Reykjavík.

Gebrande, H., H. Miller, and P. Einarsson (1980), Seismic structure of Iceland along the RRISP profile 1, *J. Geophys.*, *47*, 239–249.

Gíslason, S. R. et al. (2015), Environmental pressure from the 2014–15 eruption of Bárðarbunga volcano, Iceland, *Geochem. Perspect. Lett.*, *1*, 84–93, doi:10.7185/geochemlet.1509.

Grandin, R., E. Jacques, A. Nercessian, A. Ayele, C. Doubre, A. Socquet, D. Keir, M. Kassim, A. Lemarchand, and G. C. P. King (2011), Seismicity during lateral dike propagation: Insights from new data in the recent Manda Hararo–Dabbahu rifting episode (Afar, Ethiopia), *Geochem. Geophys. Geosyst.*, *12*(4),

©2016 American Geophysical Union. All rights reserved.

Accepted Article

doi:10.1029/2010GC003434.

Green, R. G., R. S. White, and T. Greenfield (2014), Motion in the north Iceland volcanic rift zone accommodated by bookshelf faulting, *Nature Geosci.*, *7*(1), 29–33, doi:10.1038/ngeo2012.

Green, R. G., T. Greenfield, and R. S. White (2015), Triggered earthquake suppressed by an evolving stress shadow from a propagating dyke, *Nature Geosci.*, *8*, 629–632, doi:10.1038/ngeo2491

Gudmundsson, M. T., and T. Högnadóttir (2007), Volcanic systems and calderas in the Vatnajökull region, central Iceland: Constraints on crustal structure from gravity data, *J. Geodyn.*, *43*(1), 153–169, doi:10.1016/j.jog.2006.09.015.

Hamling, I. J., A. Ayele, L. Bennati, E. Calais, C. J. Ebinger, D. Keir, E. Lewi, T. J. Wright, and G. Yirgu (2009), Geodetic observations of the ongoing Dabbahu rifting episode: New dyke intrusions in 2006 and 2007, *Geophys. J. Int., 178* (2), 989–1003, doi:10.1111/j.1365-246X.2009.04163.x.

Hartley, M. E., and T. Thordarson (2013), The 1874-1876 volcano-tectonic episode at Askja, North Iceland: Lateral flow revisited, *Geochem. Geophys. Geosyst.*, *14*(7), 2286–2309, doi:10.1002/ggge.20151.

Heimisson, E. R., A. Hooper, and F. Sigmundsson (2015), Forecasting the path of a laterally propagating dike, *J. Geophys. Res. Solid Earth*, *120*(12), 8774-8792, doi:10.1002/2015JB012402.

Hjartardóttir, Á. R., P. Einarsson, S. Magnúsdóttir, Þ. Björnsdóttir, and B. Brandsdóttir (2015a), Fracture systems of the Northern Volcanic Rift Zone, Iceland: an onshore part of the Mid-Atlantic plate boundary, *Geol. Soc. London, Spec. Publ.*, *420*, 5825, doi:10.1144/SP420.1.

©2016 American Geophysical Union. All rights reserved.

Accepted Article

Hjartardóttir, Á. R., P. Einarsson, M. T. Gudmundsson, and T. Högnadóttir (2015b), Fracture movements and graben subsidence during the 2014 Bárðarbunga dike intrusion in Iceland, *J. Volcanol. Geotherm. Res.*, doi:10.1016/j.jvolgeores.2015.12.002.

Jóhannesson, H., and K. Saemundsson (1998), Jarðfræðikort af Íslandi, *Höggun (Geological Map of Iceland. Tectonics). Náttúrufræðistofun Íslands (Icelandic Inst. Nat. Hist.), Reykjavík.*

Keir, D. et al. (2009), Evidence for focused magmatic accretion at segment centers from lateral dike injections captured beneath the Red Sea rift in Afar, *Geology*, *37*(1), 59–62, doi:10.1130/G25147A.1.

Key, J., R. S. White, H. Soosalu, and S. S. Jakobsdóttir (2011a), Multiple melt injection along a spreading segment at Askja, Iceland, *Geophys. Res. Lett.*, *38*(5), doi:10.1029/2010GL046264.

Key, J., R. S. White, H. Soosalu, and S. S. Jakobsdóttir (2011b), Correction to "Multiple melt injection along a spreading segment at Askja, Iceland," *Geophys. Res. Lett.*, *38*(10), doi:10.1029/2011GL047491.

Larsen, G., and M. T. Gudmundsson (2015), Catalogue of Icelandic Volcanoes - Bárðarbunga volcanic system, Available from: http://futurevolc.vedur.is/#

Larsen, G., M. T. Guðmundsson, P. Einarsson, and T. Thordarson (2013), *Náttúruvá á Íslandi - Eldgos og jarðskjálftar (Natural Hazards in Iceland – Eruptions and Earthquakes, in Icelandic)*, edited by S. Sólnes, F. Sigmundsson, and B. Bessason, Viðlagatrygging Íslands/Háskólaútgáfan, Reykjavík.

Lomax, A., J. Virieux, P. Volant, and C. Berge-Thierry (2000), Probabilistic Earthquake Location in 3D and Layered Models, in *Advances in Seismic Event Location*, vol. 18, edited by C. Thurber and N. Rabinowitz, pp. 101–134, Springer Netherlands.

©2016 American Geophysical Union. All rights reserved.

Accepted Article

Morita, Y., S. Nakao, and Y. Hayashi (2006), A quantitative approach to the dike intrusion process inferred from a joint analysis of geodetic and seismological data for the 1998 earthquake swarm off the east coast of Izu Peninsula, central Japan, *J. Geophys. Res. Solid Earth*, *111*(B6), doi:10.1029/2005JB003860.

Passarelli, L., E. Rivalta, S. Cesca, and Y. Aoki (2015), Stress changes, focal mechanisms, and earthquake scaling laws for the 2000 dike at Miyakejima (Japan), *J. Geophys. Res. Solid Earth*, *120*(B6), 4130–4145, doi:10.1002/2014JB011504.

Pálmason, G. (1971), *Crustal Structure of Iceland From Explosion Seismology*, Soc. Sci. Islandica, 187 pp.

Pedersen, G. B. M., A. Höskuldsson, M. S. Riishuus, I. Jónsdóttir, M. T. Gudmundsson, F. Sigmundsson, B. V Óskarsson, T. Dürig, V. Drouin, and C. Gallagher (2015), Nornahraun Lava Morphology and Emplacement: A New Terrestrial Analogue for Planetary Lava Flows, in *Lunar and Planet. Sci. Conf.*, vol. 46, p. 1845.

Peltier, A., V. Ferrazzini, T. Staudacher, and P. Bachèlery (2005), Imaging the dynamics of dyke propagation prior to the 2000–2003 flank eruptions at Piton de La Fournaise, Reunion Island, *Geophys. Res. Lett.*, *32*(22), L22302, doi:10.1029/2005GL023720.

Pugh, D. (2015), *Bayesian Source Inversion of Microseismic Events*, PhD thesis, University of Cambridge, 248 pp.

Rivalta, E., B. Taisne, A. P. Bunger, and R. F. Katz (2015), A review of mechanical models of dike propagation: Schools of thought, results and future directions, *Tectonophysics*, *638*, 1–42, doi:10.1016/j.tecto.2014.10.003.

Rubin, A. M. (1992), Dike- induced faulting and graben subsidence in volcanic rift zones, *J. Geophys. Res. Solid Earth*, *97*(B2), 1839–1858, doi:10.1029/91JB02170.

©2016 American Geophysical Union. All rights reserved.

Accepted Article

Rubin, A. M., and D. Gillard (1998), Dike-induced earthquakes: Theoretical considerations, *J. Geophys. Res. Solid Earth*, *103*(B5), 10017–10030, doi:10.1029/97JB03514.

Rubin, A. M., and D. D. Pollard (1988), Dike-induced faulting in rift zones of Iceland and Afar, *Geology*, *16*(5), 413-417, doi:10.1130/0091-7613(1988)016<0413:DIFIRZ>2.3.CO;2.

Rubin, A. M., D. Gillard, and J. L. Got (1998), A reinterpretation of seismicity associated with the January 1983 dike intrusion at Kilauea Volcano, Hawaii, *J. Geophys. Res. Solid Earth*, *103*(B5), 10003–10015, doi:10.1029/97JB03513.

Segall, P., A. L. Llenos, S.-H. Yun, A. M. Bradley, and E. M. Syracuse (2013), Time-dependent dike propagation from joint inversion of seismicity and deformation data, *J. Geophys. Res. Solid Earth*, *118*(11), 5785–5804, doi:10.1002/2013JB010251.

Sigmundsson, F. et al. (2015a), Segmented lateral dyke growth in a rifting event at Bárðarbunga volcanic system, Iceland, *Nature*, *517*(7533), 191–195, doi:10.1038/nature14111.

Sigmundsson, F. et al. (2015b), Comparison of the Bardarbunga 2014-2015 rifting event, slow caldera collapse and major effusive eruption with the 1975-1984 Krafla and 2005-2010 Dabbahu, Afar, rifting episodes., T43H-05, AGU Fall Meeting 2015, San Francisco.

Taisne, B., F. Brenguier, N. M. Shapiro, and V. Ferrazzini (2011), Imaging the dynamics of magma propagation using radiated seismic intensity, *Geophys. Res. Lett.*, *38*, 2–6, doi:10.1029/2010GL046068.

Accepted Article

©2016 American Geophysical Union. All rights reserved.

Tryggvason, E. (1984), Widening of the Krafla fissure swarm during the 1975–1981 volcano-tectonic episode, *Bull. Volcanol.*, *47*(1), 47–69, doi:10.1007/BF01960540.

Wadati, K. (1933), On the travel time of earthquake waves, *Part II, Geophys. Mag.*, *7*, 101–111.

Wright, T. J. et al. (2012), Geophysical constraints on the dynamics of spreading centres from rifting episodes on land, *Nature Geosci.*, *5*(4), 242–250.

Accepted Article

©2016 American Geophysical Union. All rights reserved.

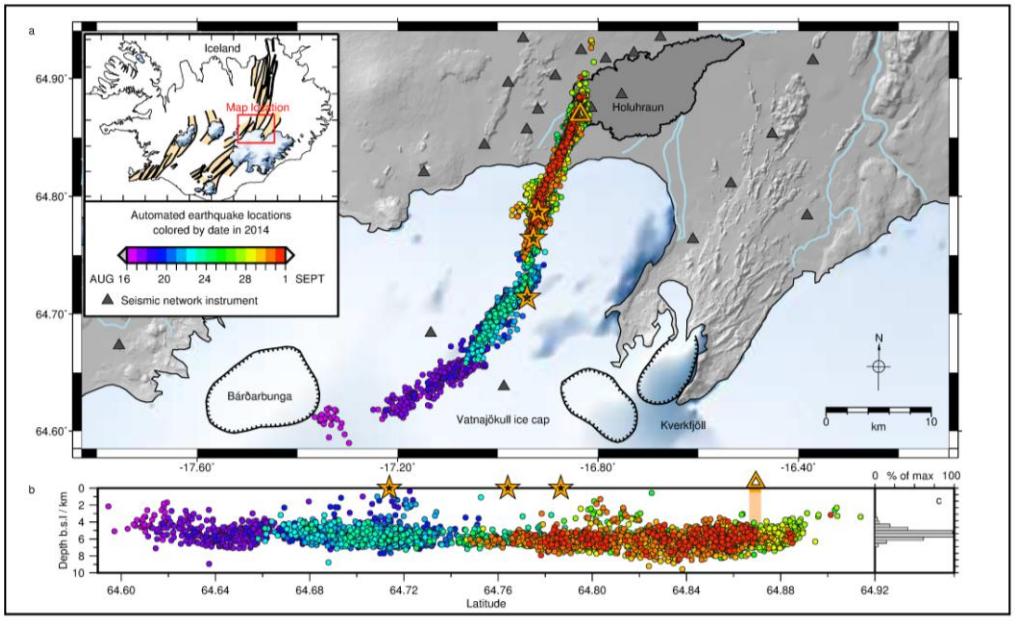

Figure 1. Seismicity produced by the propagating dike 16 - 31 August 2014, colored by date (see also Movie S1). (a) Earthquake locations in map view. Shaded topography in grey with glaciers in white. Ticked lines delineate central volcano calderas, triangles seismometers, orange triangle eruption site, stars depressions in the ice surface and dark shading new Holuhraun lava flow. Inset shows location on a simplified tectonic map of Iceland with volcanic systems shaded [*Einarsson and Saemundsson*, 1987]. (b) Cross section along dike. (c) Depth distribution of hypocenters.

Accepted Article

©2016 American Geophysical Union. All rights reserved.

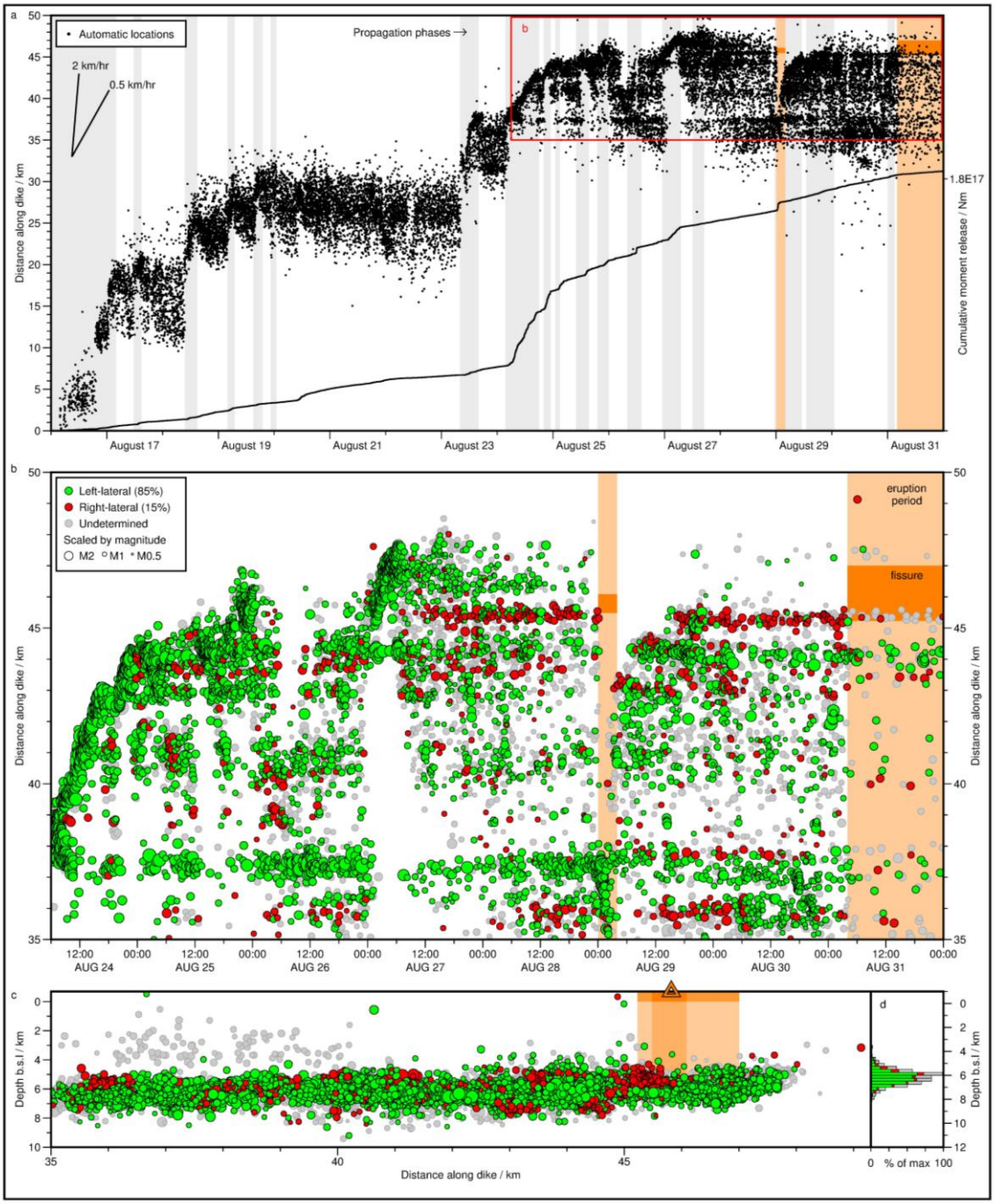

©2016 American Geophysical Union. All rights reserved.

Figure 2. Propagation of seismicity through time with earthquake failure mechanisms. (a) Automated earthquake hypocenters (black dots) delineate segmented propagation of dike, plotted as distance-along-dike versus time. Propagation phases are shown in grey. Eruption periods are shown in peach, and fissure location in orange. Dike cumulative seismic moment release is shown by solid black line. (b) Inset from (a) with left-lateral (green), right-lateral (red) and undetermined (grey) fault mechanism categorizations (see section 3.5). Earthquakes scaled by magnitude. (c) Depth cross-section of (b), with main crater identified by orange triangle. (d) Distribution of depths in (c).

Accepted Article

©2016 American Geophysical Union. All rights reserved.

Accepted Article

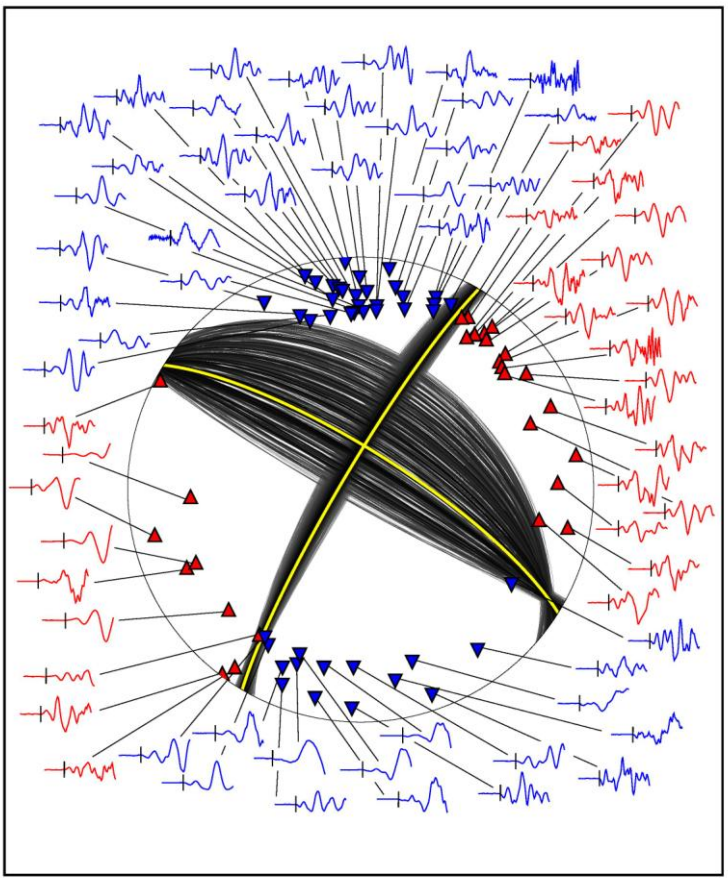

Figure 3. Example of fault plane solution with earthquake arrival waveforms. The fault plane solution is tightly constrained by polarity phase picks at 70 stations, each showing clear first motion polarity on vertical component. Each waveform is cut 0.25 s before first motion, 0.85 s in length and normalized to the same maximum amplitude. Red triangles represent compressional first motions, blue inverted triangles represent dilatational first motions. The range of possible fault plane solutions is given by the black lines, with the average fault plane solution highlighted in yellow. Location of earthquake is shown with a green star in Figure S3.

©2016 American Geophysical Union. All rights reserved.

Accepted Article

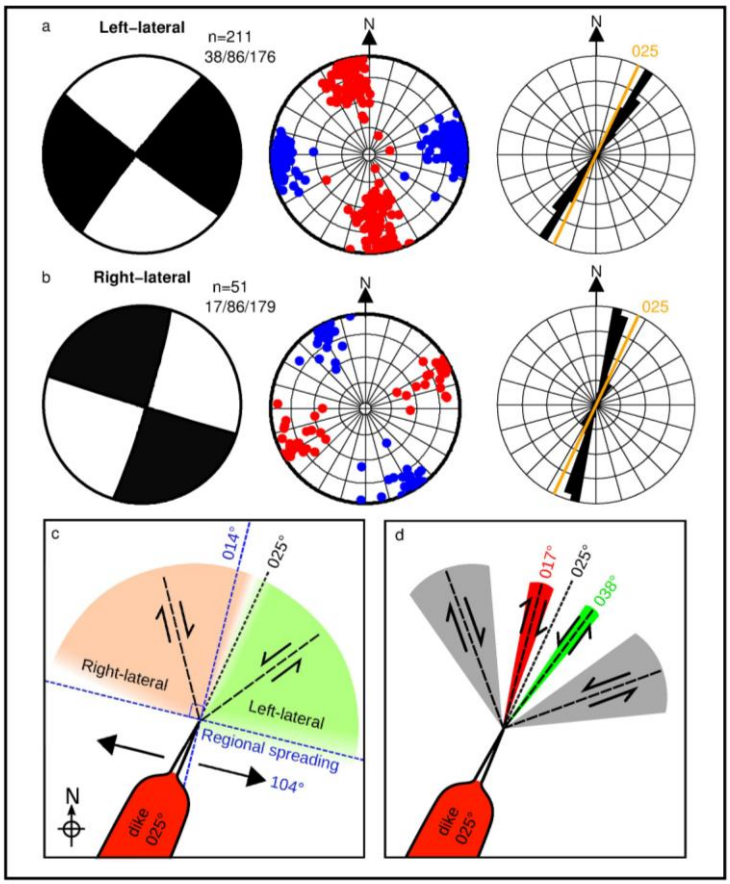

Figure 4. Fault plane solutions from northernmost segment of the dike shown in Figure 2b. Rows a–b, left to right: mean fault plane solution with strike/dip/rake marked; all P- (red) and T- (blue) axes; rose diagram of fault plane strikes, with strike of northernmost dike segment in the ice-free region in orange. (a) Left-lateral strike-slip faults. (b) Right-lateral strike-slip faults. (c) Schematic diagram showing fault motion produced by interaction of strike of dike with rift spreading direction. (d) Schematic diagram of dike tip fracture angles. *Rubin and Gillard* [1998] theoretical angles given by grey range, observed angles given by colored range. Left-lateral failure in green and right-lateral failure in red.

©2016 American Geophysical Union. All rights reserved.